NO_2-assisted molecular-beam epitaxy of wustitelike and magnetitelike Fe oxynitride films on MgO(100)

F. C. Voogt*
Department of Physical Chemistry, Materials Science Centre, University of Groningen, Nijenborgh 4, 9747 AG Groningen, The Netherlands

P. J. M. Smulders, G. H. Wijnja, and L. Niesen
Department of Nuclear Solid State Physics, Materials Science Centre, University of Groningen, Nijenborgh 4, 9747 AG Groningen, The Netherlands

T. Fujii†
Department of Solid State Physics, Materials Science Centre, University of Groningen, Nijenborgh 4, 9747 AG Groningen, The Netherlands

M. A. James and T. Hibma
Department of Physical Chemistry, Materials Science Centre, University of Groningen, Nijenborgh 4, 9747 AG Groningen, The Netherlands

(Received 4 January 2000; revised manuscript received 17 July 2000; published 13 March 2001)

In an attempt to obtain wustite $Fe_{1-x}O$ as epitaxial films on MgO(100), NO_2-assisted molecular-beam epitaxy was applied. At low NO_2 fluxes, the low-energy electron diffraction and reflection high-energy electron diffraction images indeed indicate the formation of a rocksaltlike structure. In addition, Mössbauer spectroscopy provides evidence for the formation of a phase that is paramagnetic at room temperature. However, the layers are not pure oxides but are well-ordered oxynitrides with composition $Fe_{1-x}O_{1-y}N_y$. The nitrogen atoms occupy substitutional sites on the oxygen-anion sublattice. Similarly, at slightly higher NO_2 fluxes, magnetitelike oxynitride films with composition $Fe_{3+\delta}O_{4-y}N_y$ are obtained. By correlating x-ray photoelectron spectroscopy spectra with the intensity oscillation periods observed during reflection high-energy electron diffraction, it is possible to derive the complete stoichiometry of the films. We propose that the abrupt incorporation of nitrogen atoms only occurs if the atomic oxygen provided by the NO_2 flux is insufficient to form a stoichiometric Fe_3O_4.

DOI: 10.1103/PhysRevB.63.125409 PACS number(s): 81.15.Hi, 68.55.Nq, 82.80.Pv, 82.80.Yc

I. INTRODUCTION

One of the attractive features of molecular-beam epitaxy (MBE) is that, by proper choice of substrate and growth conditions, thermodynamically metastable and unstable phases can sometimes be prepared in the form of thin films. In two previous publications, we have already demonstrated that the technique of NO_2-assisted MBE is not only capable of inducing the stable magnetite Fe_3O_4,[1] and hematite α-Fe_2O_3,[2] phases but also the metastable maghemite γ-Fe_2O_3 phase. Furthermore, it was even possible to obtain all nonstoichiometric $Fe_{3-\delta}O_4$ phases in between Fe_3O_4 and γ-Fe_2O_3.[1] In this complementary paper, we report on the formation and properties of iron oxides with low-oxidation states, i.e., reduced magnetite and especially, wustite.

Wustite is thermodynamically only stable above 833 K. Below this temperature, it tends to disproportionate into α-Fe and Fe_3O_4. It is an antiferromagnet with a Néel temperature of $\sim$200 K that, however, strongly depends on the deviation from the ideal 1:1 stoichiometry.[3] Although very rare as a mineral, it is believed to be a major constituent of the earth's core. Therefore, it is an important subject of study in geology. Wustite adopts the very common rocksalt crystal structure of NaCl with a lattice constant of approximately 0.43 nm.[4]

Its formula unit, $Fe_{1-x}O$, indicates that wustite is a nonstoichiometric compound; there are vacancies located on the Fe^{2+} sublattice. Each of them is accompanied by the conversion of two Fe^{2+} ions to Fe^{3+} in order to maintain charge neutrality. The fraction of Fe ranges from 0.97 to 0.84.[5] From neutron and x-ray diffraction studies and also from calculations, it has been deduced that nonstoichiometric wustite contains defect clusters.[6] The simplest of defect clusters is formed by an interstitial Fe^{3+} ion on a tetrahedral site, surrounded by four vacancies on neighboring octahedral sites. Together, they are arranged in a tetrahedron. This is a so-called 4:1 cluster (four vacancies, 1 interstitial). The negatively charged core of this cluster is surrounded by a positive shell, which contains substitutional Fe^{3+} ions on octahedral sites. This basic 4:1 unit can form larger aggregates via edge or corner sharing of the tetrahedrons, leading to higher-order clusters such as 8:3, 10:4, 16:5, etc. The best known defect cluster is the 13:4 Koch-Cohen cluster.[7] Interestingly, these defect clusters locally resemble the structure of Fe_3O_4. Therefore, they are believed to act as nucleation sites during the disproportionation or oxidation of $Fe_{1-x}O$ to Fe_3O_4. However, there is no continuous range of phases between these two oxides in contrast to Fe_3O_4 and γ-Fe_2O_3.[1]

Thus far, there have been very few reports of MBE-grown

$Fe_{1-x}O$ films in contrast to Fe_3O_4 and α-Fe_2O_3. In conventional O_2-assisted MBE, one encounters a discontinuous jump from Fe_3O_4 to unoxidized, metallic α-Fe at low O_2 partial pressures.[8–10] This reflects the thermodynamic instability of $Fe_{1-x}O$. On some occasions, Fujii *et al*. did observe traces of $Fe_{1-x}O$ but these results were not reproducible.[8] Only recently, Ruby *et al*. managed to prepare $Fe_{1-x}O$/MgO(100) films using extremely low Fe deposition rates and O_2 partial pressures.[11] However, these films were highly unstable; they rapidly oxidized even at room temperature under residual vacuum pressures. Vurens *et al*. succeeded in preparing stable epitaxial FeO overlayers on Pt(111) but only with a thickness of one atomic monolayer (ML).[12,13] Thicker films had the stoichiometry of Fe_3O_4 or α-Fe_2O_3.[14,15] However, it appears that it is possible to grow thick, bulklike wustite layers if conditions are chosen that are further away from equilibrium. Thus far, a few research groups obtained polycrystalline material on amorphous substrates by applying pulsed laser deposition[16] or reactive rf magnetron sputtering.[17–19] There has been one report of single-crystalline, epitaxial $Fe_{1-x}O$/MgO(100) films by Gao *et al*. who used O_2-plasma-assisted MBE.[20] However, there were indications that the surfaces of the as-grown films rapidly transformed to Fe_3O_4 due to postoxidation. Again, this reflects wustite's instability.

In this light, our technique of NO_2-assisted MBE has two promising features. First, studies by Voogt *et al*.[1] have shown that NO_2 is a very efficient oxidizing agent. To induce the formation of stoichiometric Fe_3O_4 films, it is enough that the fluxes of Fe and NO_2 are of the same magnitude. This indicates that the oxidation process is to a large extent kinetically controlled, i.e., the conditions are far away from equilibrium. We thus can expect the formation of $Fe_{1-x}O$ if the ratio of NO_2 and Fe fluxes is set at $\sim 1:1$. Second, since the NO_2 is provided in the form of a molecular beam and only small doses are needed to fully oxidize the metal deposits, the background pressure during deposition can be maintained in the near-ultra-high vacuum (UHV) region, i.e., 10^{-8}–10^{-7} Torr. Therefore, not only the deposition but also the oxidation process can abruptly be stopped, i.e., we can avoid postoxidation.

In this paper, we demonstrate that wustite films indeed can be prepared. However, these films are not pure oxides; they are oxynitrides. The substitution of part of the oxygen-anion sublattice with nitrogen atoms probably facilitates stabilization of this phase. At slightly larger NO_2 fluxes, similar magnetitelike oxynitride phases are obtained. The incorporation of nitrogen might open up the possibility to mimic other (mono)oxides not existing in bulk form. Preliminary results have already indicated the successful formation of a CrO ''look-alike.''[21] Furthermore, these oxynitride films may also be important for studies on corrosion as similar phases have been observed after oxidation of nitrided Fe films.[22]

II. EXPERIMENT

The experimental setup and method have already been described in detail in a previous publication.[1] Here, we briefly recall the essential features. All samples have been grown in a standard UHV-MBE system equipped with facilities for reflection high-energy electron diffraction (RHEED), low-energy electron diffraction (LEED), and x-ray photoelectron spectroscopy (XPS) using nonmonochromatic Al K_α radiation and Auger electron spectroscopy (AES). The base pressure of the system is in the low 10^{-10} Torr region. After characterization *in situ*, the samples were also examined *ex situ* using conversion electron Mössbauer spectroscopy (CEMS), Rutherford backscattering spectroscopy (RBS), and x-ray diffraction (XRD).

Sample films were grown by depositing metals from effusion cells onto oxygen-annealed *ex situ* cleaved MgO(100) substrates. By simultaneously exposing the metal deposits to a beam of NO_2 molecules, oxide films were formed. The NO_2 molecules came from a small buffer volume via a stainless steel pipe directed at the substrate surface. By varying the buffer volume pressure, P_{buf}, the flux of NO_2 molecules and therewith, the degree of oxidation can be controlled.

As substrate, MgO(100) was chosen because it has the same cubic rocksalt crystal structure as wustite. The similar lattice constants of MgO and $Fe_{1-x}O$, i.e., 0.421 12 and $\sim$0.43 nm,[4] respectively, result in a modest mismatch of only 2%, thus favoring coherent, single-crystalline epitaxial growth. The deposition rate of Fe (natural or enriched in ^{57}Fe), measured by moving a quartz crystal micro balance in the position of the substrate, was set at 0.13 nm/min with the substrate temperature set at 525 K. Under these conditions, we know from our previous studies[1] that the minimum P_{buf} value needed to induce the formation of stoichiometric Fe_3O_4 equals 0.75 mTorr. Therefore, we varied P_{buf} from 0.75 down to 0.20 mTorr. Our samples consisted of a 20.0 nm iron-oxide layer grown with ^{57}Fe, sandwiched between two 5.0 nm buffer and caplayers grown with natural Fe. Thus, we obtained films with a total thickness of 30.0 nm with one oxidation state all over but with Mössbauer inactive surface and interface regions, i.e., our CEMS spectra represent the bulklike interior. The XPS spectra have been measured on the ^{57}Fe probe layer, before deposition of the cap layer, in order to allow a direct comparison with the CEMS spectra.

III. RESULTS AND DISCUSSION

A. RHEED and LEED observations

With RHEED (and LEED), it is straightforward to discriminate between wustite and the other iron-oxide phases. Both MgO and $Fe_{1-x}O$ have the rocksalt crystal structure and, therefore, give rise to similar diffraction patterns. In contrast, Fe_3O_4(100) and γ-Fe_2O_3(100) are known to display more complex patterns.[1,23] The hexagonal α-Fe_2O_3 does not have an epitaxial relationship with MgO(100). Thus, simply by observing the RHEED screen during deposition, the conditions necessary to induce the formation of wustite can be determined.

Initially, an iron-oxide film was deposited on MgO(100) at 525 K using a buffer pressure of 0.75 mTorr and an Fe flux of 0.13 nm/min. As shown in Fig. 1(b), the RHEED diffraction pattern of the magnetite (inverse) spinel structure,

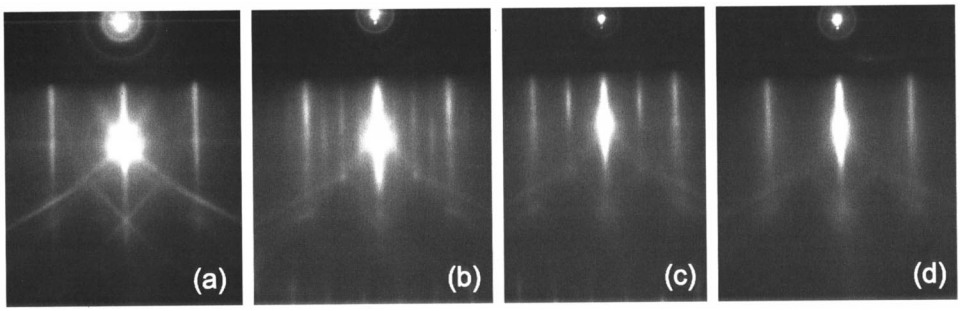

FIG. 1. RHEED patterns recorded at an electron energy of 15 keV with the beam incident along a [100] direction. (a) A MgO(100) substrate, cleaved *ex situ* and annealed *in situ* under 10^{-6} Torr of O_2 at 975 K for 2–3 h. (b) An epitaxial $Fe_3O_4(100)$ film with a $(\sqrt{2}\times\sqrt{2})R45°$ reconstruction ($P_{buf}=75$ mTorr). (c) An unreconstructed $(1\times1)Fe_3O_4(100)$ surface ($P_{buf}=40$ mTorr). (d) An unreconstructed $(1\times1)Fe_{1-x}O(100)$ surface ($P_{buf}=35$ mTorr). By comparing with (a), it can be seen that this pattern has the same rocksalt-symmetry as MgO(100).

including the extra diffraction lines due to the $(\sqrt{2}\times\sqrt{2})R45°$ reconstruction, was observed. Then, the NO_2 flux was reduced while keeping the Fe flux constant.

When the NO_2 had dropped below 0.60 mTorr, the RHEED pattern changed markedly. First, the $(\sqrt{2}\times\sqrt{2})R45°$ lines started to fade away until at a buffer pressure of 0.40 mTorr only an unreconstructed (1×1) magnetite pattern remained; see Fig. 1(c). At even lower fluxes, a diffraction pattern appeared that was consistent with a cubic rocksalt structure [Fig. 1(d)]. For comparison, a RHEED pattern of a clean and well-ordered MgO(100) substrate is shown in Fig. 1(a). The similarity of the patterns indicates that the latter films consist of a wustitelike material.

This is confirmed by LEED. In Fig. 2(a), the LEED pattern is shown of an iron-oxide film prepared at 35 mTorr. This pattern displays the same square symmetry and periodicity as those of a clean and well-ordered MgO(100) substrate [see Fig. 2(b)] suggesting that an unreconstructed (1×1) $Fe_{1-x}O$ surface has been formed. In contrast, Gao *et al.*[20] observed a (2×2) reconstruction. This was attributed to an ordered arrangement of 4:1 defect clusters at the surface. However, we point out that a (1×1) rocksalt pattern is a much stronger evidence for the formation of wustite than a (2×2) rocksalt pattern, because the latter cannot easily be distinguished from a (1×1) spinel pattern. Since the as-grown samples of Gao *et al.* were suspended for a few minutes in an O_2 background pressure while cooling down, it is, therefore, more likely that their $Fe_{1-x}O(100)$ surfaces were simply postoxidized to unreconstructed $Fe_3O_4(100)$. On the other hand, a (1×1) rocksalt pattern would correspond to a $(\frac{1}{2}\times\frac{1}{2})$-reconstructed $Fe_3O_4(100)$ pattern. Such a reconstruction has only once been reported, by Gaines *et al.*[24] It is telling that scanning-tunneling microscopy revealed that this surface actually consisted of unreconstructed FeO(100).[24]

B. XPS analysis

In order to make a systematic study of the above findings, a series of samples were prepared as described in Sec. II. The RHEED and LEED patterns of these samples were in agreement with the above observations. Considering the stoichiometry, the samples were first characterized with XPS. In Fig. 3, the spectra of the Fe $2p$ core levels are shown, as a function of the NO_2 flux during growth. All samples were charging to varying extents during the XPS measurements.

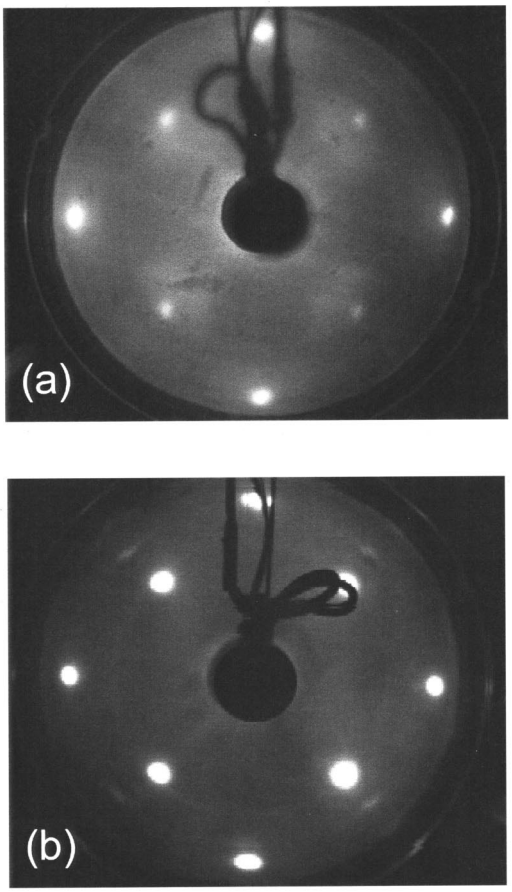

FIG. 2. (a) LEED pattern, corresponding to the RHEED pattern displayed in Fig. 1(d): an unreconstructed (1×1) $Fe_{1-x}O(100)$ surface ($P_{buf}=35$ mTorr). The pattern was recorded at an electron beam energy of 84 eV. (b) For comparison, a LEED pattern of a clean MgO(100) substrate is included (recorded at an electron energy of 85 eV). This pattern corresponds to the RHEED pattern displayed in Fig. 1(a). The periodicity and symmetry of the two LEED patterns are similar.

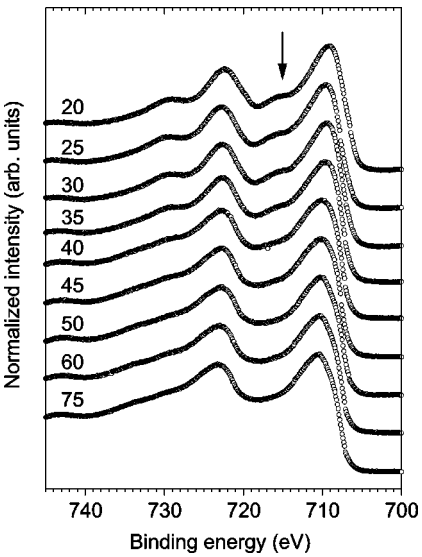

FIG. 3. XPS spectra (Al $K\alpha$) of the Fe $2p$ core levels as a function of the NO_2 buffer volume pressure applied during deposition. The number on the left-hand side in each spectrum is the pressure in mTorr. All spectra have been corrected for charging by assuming an O $1s$ BE of 530.1 eV. The arrow in the top spectrum indicates the position of the Fe^{2+} satellite peak at ~716 eV.

This has been taken into account by putting the binding energy (BE) of the O $1s$ core levels at 530.1 eV.[25]

The spectrum of the 0.75 mTorr sample corresponds to stoichiometric Fe_3O_4. This is confirmed by the CEMS spectrum.[1] We refer to Ref. 25 for a detailed discussion of the Fe $2p$ line shape. In short, a spectrum of Fe_3O_4 consists of superposition of Fe^{2+} and Fe^{3+} spectra because magnetite is a mixed-valency compound. Ferric ions in Fe_2O_3 have a BE of 711.0 eV for the main Fe $2p_{3/2}$ line, and ~719 eV for the satellite peak. For the Fe^{2+} ions in $Fe_{1-x}O$, these values are 709.5 and ~716 eV, respectively. As can be seen in Fig. 4, for the 0.75-mTorr sample, a superposition of these spectra leads to a broadened main line and a smeared-out satellite structure. For the main line, we find a BE of 710.4 eV, which agrees well with literature values (710.5 eV).

When the NO_2 flux is lowered, the weight of the Fe^{3+} component in the XPS spectra reduces. In Fig. 3, it can be seen that the BE of the Fe $2p_{3/2}$ main line stays at 710.3 eV

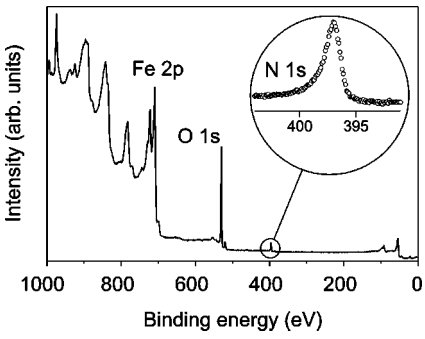

FIG. 4. Al $K\alpha$ XPS broad scan of the $Fe_{1-x}O$ film prepared at $P_{buf}=0.35$ mTorr. The inset shows an enlargement of the N $1s$ core level region around 397.0 eV.

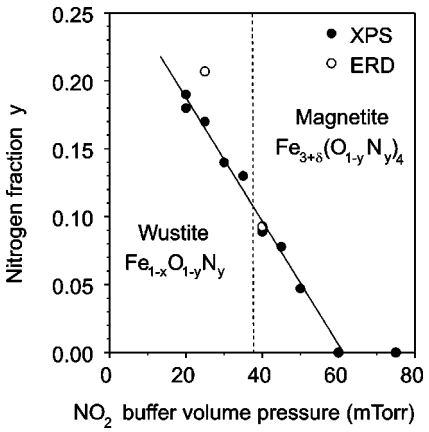

FIG. 5. The nitrogen content of samples grown at low NO_2 fluxes as determined from XPS spectra (filled circles) and ERD measurements (open circles). The dotted line separates the magnetite and wustite single-phase regions. The solid line through the data points indicates the linear increase in nitrogen content with decreasing NO_2 flux.

down to 0.40 mTorr. At 0.35 mTorr, the line shifts to lower energies, i.e., 709.5 eV. Now, also the Fe^{2+} satellite at ~716 eV becomes visible. Upon further reduction of the NO_2 flux, the satellite becomes more pronounced, and the main line shifts gradually to 709.2 eV. We point out that the change in the XPS spectra coincides with the change in the RHEED and LEED patterns from spinellike structures to rocksaltlike structures. Therefore, these results give supplementary evidence that between 0.40 and 0.35 mTorr, there is a change in phase from Fe_3O_4 to $Fe_{1-x}O$. Between 0.75 and 0.40 mTorr Fe has a valency as in Fe_3O_4, but at 0.35 mTorr the valency changes to predominantly Fe^{2+}, as in $Fe_{1-x}O$, although there is still an Fe^{3+} fraction present. Going down to 0.20 mTorr, this Fe^{3+} fraction further decreases and the Fe^{2+} features become clearer. As a matter of fact, between 0.35 and 0.20 mTorr, the spectra are very similar to that of ilmenite $FeTiO_3$, one of the few oxides with only ferrous Fe^{2+} ions.[26]

Most importantly, we find that all samples prepared at NO_2 buffer pressures below 0.60 mTorr contain nitrogen. Figure 4 shows an XPS broad scan of the 0.35 mTorr sample. Besides the Fe and O lines, there is a clear peak at 397.0 eV corresponding to the N $1s$ core level. This contamination with nitrogen is confirmed by AES spectra (not shown), RBS (see below), and by elastic-recoil detection (ERD). ERD is an ion-scattering technique capable of discriminating between light elements in a heavier matrix.[27] To determine the nitrogen content relative to the oxygen content, we compared the areas under the N $1s$ and O $1s$ core level peaks. This was done after subtracting a Shirley-type background and correcting for the difference in ionization cross sections.[28] In Fig. 5, we have plotted the results as a function of the NO_2 pressure. For comparison, two data points obtained with ERD have been added. These values agree well with the ones from XPS.

It can be seen that all magnetite phases grown at NO_2 pressures larger than 0.60 mTorr are free from nitrogen. That is, the content is below the detection limit of the XPS appa-

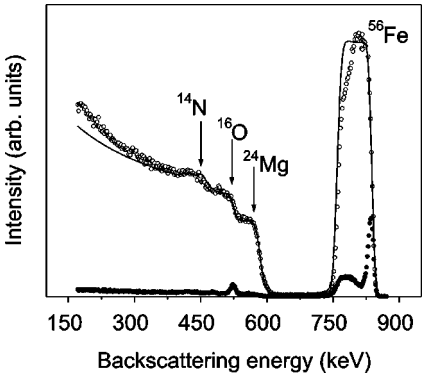

FIG. 6. RBS spectra of the $Fe_{1-x}O$/MgO(100) film prepared at $P_{buf}=0.35$ mTorr. Open circles: ion beam incident at a random direction. Filled circles: ion beam incident along the [100] surface normal. The solid line is a simulated spectrum for a 30.0-nm-thick film with a $Fe_{0.82}O_{0.82}N_{0.18}$ composition. The arrows indicate the position of the Mg, O, and N edges.

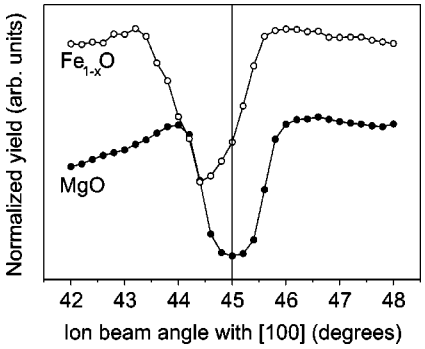

FIG. 7. RBS channeling dips in the [110] direction for a MgO(100) substrate (open circles) and an $Fe_{1-x}O$ epitaxial film prepared at $P_{buf}=0.35$ mTorr (filled circles). For the film, the dip is shifted over 0.6(1)° indicating compressive stress.

ratus, which is of the order of a few percent of a ML. However, at 0.55 mTorr, the nitrogen suddenly appears and its content increases linearly with decreasing NO_2 flux, up to $\sim$20% at 0.20 mTorr.

The XPS BE of 397.0 eV for the N 1*s* core level is typical of a nitride species. It excludes the presence of nitrate $(NO_3)^-$ or nitrite $(NO_2)^-$ ions, etc., since nitrogen has a much higher BE in these environments.[29] However, the presence of simple Fe_xN nitrides can also be excluded. The BE of the Fe $2p_{3/2}$ core level in these phases is very close to that in the metallic state, e.g., 707.3 eV in ξ-Fe_2N,[30] whereas we find values of 709.5–709.2 eV that are typical for Fe^{2+} in $Fe_{1-x}O$. Furthermore, all techniques applied to the samples, including XRD, RBS, and CEMS (see below), indicate that the samples are single-phase crystals. These facts, and the finding that the nitrogen uptake is nearly linear with decreasing NO_2 flux, can only be explained if the nitrogen is incorporated in the layers by replacing part of the oxygen atoms. In other words, the present samples are single-crystalline oxynitrides.

The only exception is the 0.20 mTorr sample. In this particular case, the Fe $2p_{3/2}$ is broadened towards lower BE. Furthermore, the N 1*s* line is broadened towards higher BE and the CEMS spectra indicates a higher Fe^{3+} content than in the other wustite samples (see below). Therefore, this sample seems to consist of a poorly ordered mixture of multiple phases.

C. RBS and XRD analysis

From the RHEED and LEED patterns, it follows that the films grow epitaxially on MgO(100). To analyze the epitaxy and crystal structure of the films in a more quantitative way, we performed a combined RBS and XRD analysis. XRD θ-2θ scans only show diffraction peaks that nearly coincide with the (002) and (004) peaks of the MgO substrate. This supports the proposition that the films have a rocksalt or spinel crystal structure. There are no peaks corresponding to other phases. In the remainder of this section, we focus on the wustite sample prepared at $P_{buf}=0.35$ mTorr NO_2. Two RBS spectra of this sample are shown in Fig. 6: one with a random direction of the ion beam (open circles) and one where the beam was channeled along the [100] surface normal (filled circles). The minimum yield in the channeling direction is reasonably low ($\leqslant$10%) indicating a good crystalline structure with few defects. Besides [100], also the $\langle 110\rangle$ and $\langle 111\rangle$ channeling directions of the film approximately coincide with those of the substrate. This confirms the $Fe_{1-x}O(100)\|MgO(100)$ and $Fe_{1-x}O[001]\|MgO[001]$ epitaxial relationships.

The RBS measurements confirm the XPS result that the film contains nitrogen. There is a clear edge, corresponding to the ^{14}N isotope, superimposed on the Mg and O edges. The random spectrum can be fairly well reproduced by a simulation for a 30-nm-thick film with a $Fe_{0.45}O_{0.45}N_{0.10}$ composition. The relative nitrogen and iron contents from RBS are in reasonable agreement with the XPS data and the RHEED intensity oscillation periods (see Secs. III B and III E). We point out that the wustite sample is remarkably stable: even when exposed to air, there is no sign of oxidation to a magnetitelike phase. Interestingly, the minimum yield in the channeling direction for *N* is of the same order of magnitude as for Fe, O, and Mg. Again, this indicates that *N* is not randomly distributed but instead occupies regular lattice sites.

To detect the presence of epitaxial strain in the film, the [110] axis channeling angle was measured. This angle was determined by scanning the ion beam through the (001) crystal plane, from the [100] surface normal to the in-plane [010] axis, until a minimum was found for the Fe signal. For reference, we used the channeling dip in the O signal of the MgO substrate. This was done by performing a separate scan on a part of the sample that was shadowed by the tantalum strips during deposition.

The two channeling dips are shown in Fig. 7. Plotted is the normalized yield as a function of the angle of incidence of the ion beam with respect to the surface normal for the MgO substrate (filled circles) and the iron-oxide thin film (open circles). It is found that the [110] axis of the film is slightly tilted towards a more out-of-plane direction. For the MgO substrate, the angle between the [100] and [110] axes is

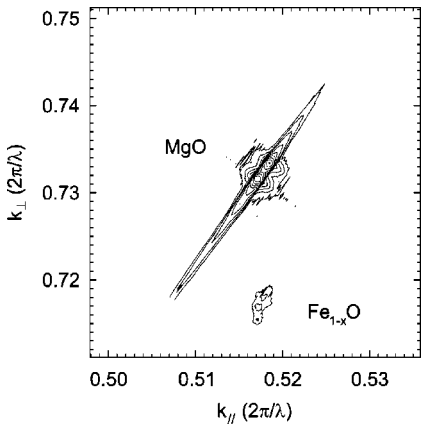

FIG. 8. XRD map of the reciprocal space around the nonspecular (224) reflection of a 30.0-nm-thick $Fe_{1-x}O$/MgO(100) film prepared at $P_{buf}=0.35$ mTorr. Plotted is the logarithm of the diffracted intensity as a function of the in-plane $k_\parallel$ and out-of-plane $k_\perp$ reciprocal wave vectors. The x and y axes are in units of $2\pi/\lambda$ with $\lambda = 0.154\,18$ nm.

exactly 45°, as expected for an undistorted cubic crystal. For the $Fe_{1-x}O$ film, this angle deviates from 45° by 0.6(1)°. This tetragonal distortion shows that there is epitaxial strain. Since the tilt is towards the surface normal, it follows that the film is compressed in-plane. For measurements of Fe_3O_4 (Refs. 24 and 31–33) and γ-Fe_2O_3 (Ref. 33) films, it has always been found that the overlayers were expanded.

To determine whether the growth is fully coherent or partly relaxed, an XRD analysis was performed as well. A two-dimensional map of the reciprocal space around the (224) reflection is shown in Fig. 8. The map was constructed by performing several ω scans for increasing values of θ. Note that the intensity scale is logarithmic. There are two groups of features: a bright one corresponding to the MgO substrate and a much weaker one, at smaller $k_\perp$ values, corresponding to the $Fe_{1-x}O$ thin film. In both cases, the features consist of two peaks, originating from Cu $K\alpha_1$ and $K\alpha_2$ radiation, which are superimposed on a low-intensity elongated streak, originating from remnant white radiation. The fact that the peaks of MgO and $Fe_{1-x}O$ are at the same $k_\parallel$ values directly proves that the film is fully coherent. This finding is consistent with the observation of a two-dimensional layer-by-layer growth mode (see Sec. III E) instead of a three-dimensional Stranski-Krastanov growth mode. Furthermore, its smaller $k_\perp$ value confirms that the film is indeed compressed in-plane.

Using MgO's lattice constant of 0.421 12 nm for normalization, an out-of-plane lattice constant of 0.4298(5) nm is determined. Combined with the in-plane spacing, this results in a tilt of the [110] direction of 0.58°, in good agreement with the RBS measurement. In the case of a three-dimensional isotropic system with in-plane stress, the relationship between the in-plane strain ϵ_i and the out-of-plane strain ϵ_o is given by[34]

$$\epsilon_o = \frac{-2\nu}{1-\nu}\epsilon_i,$$

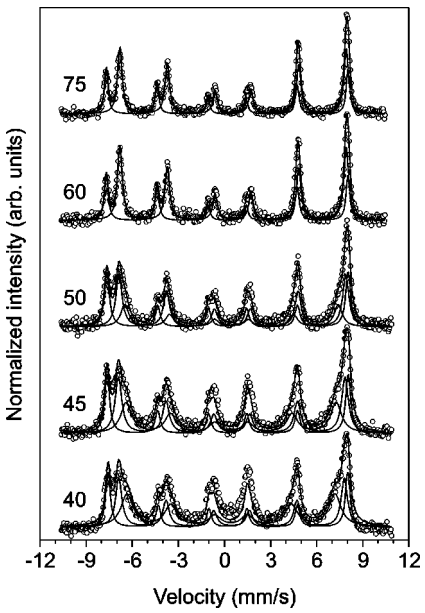

FIG. 9. Room-temperature CEMS spectra of the magnetite samples (open circles), prepared with low fluxes of NO_2. The buffer volume pressure (in mTorr) is indicated on the left-hand side of each spectrum. The 0.75- and 0.60-mTorr spectra have been fitted with three components (solid lines); the others with two.

where ν is the Poisson ratio of the material. Assuming a similar Poisson ratio as for pure wustite, i.e., 0.364,[35] we find that the unstrained bulk lattice parameter of our material is equal to 0.4252(5) nm. This value is outside the range of 0.427 74–0.431 08 nm reported for pure $Fe_{1-x}O$.[4] Apparently, the lattice has shrunk because of the substitution of oxygens by smaller nitrogen atoms.

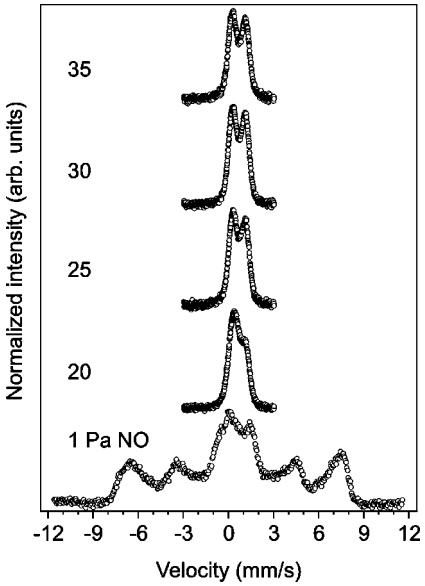

FIG. 10. Room-temperature CEMS spectra of the wustite samples prepared with low fluxes of NO_2. The buffer volume pressure (in mTorr) is indicated on the left-hand side of each spectrum. The bottom spectrum is of a sample prepared at 10.00 mTorr NO.

TABLE I. Fit parameters of the two- and three-component fits to the 0.75–0.40 mTorr NO_2 samples. Listed are the hyperfine field (HF), and the isomer shift (IS) relative to α-Fe, the measured fractions of the various components, and calculated fractions based upon a binomial distribution of oxygen and nitrogen neighbors in accordance with the XPS data.

$p(NO_2)$ (mTorr)	Component	*HF* (T)	*IS* (mm/s)	Measured fraction	Calculated fraction
0.75	$Fe^{2.5+}$	45.67(2)	0.664(3)	0.66(2)	
	Fe^{3+}	48.76(2)	0.282(3)	0.34(2)	
0.60	$Fe^{2.5+}$	45.67(2)	0.663(3)	0.67(2)	
	Fe^{3+}	48.74(3)	0.283(4)	0.33(2)	
0.50	$Fe^{2.5+}$	45.75(6)	0.621(6)	0.44(4)	0.499
	Fe^{3+}	48.67(4)	0.305(6)	0.33(2)	0.275
	Fe-N	43.1(2)	0.56(2)	0.23(4)	0.226
0.45	$Fe^{2.5+}$	45.70(7)	0.578(6)	0.38(4)	0.410
	Fe^{3+}	48.64(4)	0.314(6)	0.27(2)	0.241
	Fe-N	42.3(2)	0.55(2)	0.35(4)	0.350
0.40	$Fe^{2.5+}$	45.5(1)	0.57(1)	0.32(5)	0.381
	Fe^{3+}	48.37(6)	0.329(9)	0.25(3)	0.230
	Fe-N	41.9(3)	0.53(2)	0.43(6)	0.389

D. Mössbauer spectroscopy

In Fig. 9, the room-temperature CEMS spectra of the 0.60–0.40 mTorr samples, and in Fig. 10, those of the 0.35–0.20 mTorr samples are shown. For comparison, the spectrum of a sample grown with 10.00 mTorr NO (nitrogen monooxide) as the oxidizing agent, is included at the bottom of Fig. 10. This spectrum will be discussed in Sec. IV. The spectra of the 0.60–0.40 mTorr samples are typical for magnetite.[1] However, for lower fluxes, there is an abrupt change: the spectra of the 0.35–0.20 mTorr samples show structures that are composed of paramagnetic doublets. A paramagnetic behavior at room temperature is characteristic for wustite,[36] because of its low Néel temperature of around 200 K.[3] At temperatures of 80–100 K, the CEMS spectra of the 30 and 35 mTorr samples indeed display sextet structures,[37] indicating wustitelike phases below their Néel temperature. The doublet structures in the paramagnetic room-temperature spectra are the result of the interaction between the ^{57}Fe nuclear quadrupole moment and an electrical field gradient at the nucleus. This gradient is caused by the vacancies, nitrogen atoms, and Fe^{3+} interstitials present in the otherwise cubic rocksalt crystal lattice.

The spectra of the 0.75 and 0.60 mTorr can satisfactorily be fitted with two components corresponding to Fe^{3+} and $Fe^{2.5+}$ ions (we refer to Ref. 1 for a detailed description of the CEMS analysis). The resulting value for δ, the number of Fe vacancies per formula unit, is equal to 0 within the error limits showing that these samples are stoichiometric Fe_3O_4. However, the other magnetite spectra need to be fitted with at least three components. For instance, in the spectra of the 0.45 and 0.40 mTorr samples, there is a clear shoulder on the left-hand side of the peak at +8 mm/s. Since the XPS data suggested that part of the oxygen sublattice is replaced by nitrogen, we attribute the third component to Fe ions that have at least one nitrogen nearest neighbor.

In Table I, the results of the two- and three-component fits to the magnetite spectra are listed. The fits did not include a quadrupole splitting since the inclusion of this parameter did not reduce the error sum significantly. We point out that even with three components the spectrum of the 0.40 mTorr sample is still not fitted very well, especially the inner two lines. The higher intensity at this position suggests the onset of a paramagnetic fraction similar to the spectrum of the 10.00 mTorr NO sample.

To analyze these spectra, it is assumed that the nitrogen atoms are distributed randomly over the anion sublattice. In this case, the probability P that an Fe atom has n_1 nitrogen and n_2 oxygen neighbors follows a binomial distribution

$$P_N(n_1) = \frac{N!}{n_1! n_2!} p^{n_1} q^{n_2},$$

where N is the total number of neighbors (4 and 6 for tetrahedral and octahedral irons, respectively). Furthermore, p is the chance that a particular neighbor site is occupied by a nitrogen. This chance is equal to the nitrogen fraction as determined by XPS. If the site is not occupied by nitrogen, it must be occupied by an oxygen and hence, this chance q is equal to $1-p$.

In the case of the 0.50 mTorr sample, $p=0.047$, so $q=0.953$. Therefore, the probability that an octahedral Fe is surrounded by oxygens only, i.e., $n_1=0$ and $n_2=6$, is equal to 0.749. Similarly, the probability that a tetrahedral Fe is surrounded by oxygens only is equal to 0.825. All other Fe atoms are surrounded by at least one (or more) nitrogens. Considering that the ratio of octahedral to tetrahedral Fe atoms in stoichiometric magnetite is 2, the fractions that are listed in Table I are found for the three types of iron. These calculations have been repeated for the 0.45 and 0.40 mTorr samples. It can be seen that there is a fairly good agreement between the calculated and measured fractions. This gives confidence for the attribution of the third component to nitrogen-surrounded irons and therewith, for the assumption that nitrogen occupies substitutional sites on the oxygen sublattice.

The wustite spectra can satisfactorily be fitted with two or three quadrupole-split doublets. Because of the complexity of the samples, it is not possible to make an unambiguous attribution of these components to specific Fe sites. The centers of gravity of the four spectra are at isomer shifts of 0.73, 0.73, 0.74, and 0.67 mm/s for the 0.35–0.20 mTorr samples, respectively. If we assume isomer shifts of 0.30 and 1.0 mm/s for Fe^{3+} and Fe^{2+} ions,[36] respectively, then we find Fe^{3+} fractions of 0.39, 0.39, 0.37, and 0.47 for the 0.35–0.20 mTorr samples.

E. Stoichiometry from RHEED intensity oscillation periods

During deposition of the oxynitride films, oscillations are observed in the intensity of the specularly reflected RHEED beam.[38] It is well established that these oscillations indicate a two-dimensional or Frank-van der Merwe growth mode.[39–41] The period of the oscillations corresponds to the formation time of one new layer.

As mentioned in the Introduction, wustite crystallizes in the rocksalt structure. Viewed along the [100] growth direction, this structure consists of fcc close-packed (100) oxygen planes with all the intermediate octahedral sites filled with Fe^{2+} cations. There are two such charge-neutral planes per unit cell with interplanar distances of 0.21 nm. The spinel crystal structure is slightly more complex. It also is based upon fcc close-packed (100) oxygen planes; the so-called *B* planes. However, here only half of the octahedral sites are filled; the remaining cations are in tetrahedral sites. These tetrahedral sites form planes halfway between the *B* planes; the so-called *A* planes. Nevertheless, a charge-neutral stacking repeat unit (an *A*-*B* bilayer) also has a thickness of 0.21 nm.

In previous studies,[1,38,42] we have devided the total film thickness, as derived from XRD and RBS measurements, by the number of RHEED oscillations observed during deposition. It was found that for all cubic iron oxides (γ-Fe_2O_3, Fe_3O_4, and $Fe_{1-x}O$), layer-by-layer growth proceeds with 0.21-nm-thick units. This directly proves that each growth layer comprises of only one oxygen monolayer together with the appropriate amount of cations to maintain charge neutrality. In the wustite structure, the latter is simply achieved by filling all the octahedral sites; in the spinel structure, however, growth has to proceed with the simultaneous advance of *A* and *B* layers. As a matter of fact, we always observe the well-known $(\sqrt{2}\times\sqrt{2})R45°$ reconstruction during deposition of $Fe_3O_4(100)$ films.[1,2,3] This shows that Fe_3O_4 grows with *trilayers*, namely, a complete *B* layer with two *half-filled A* layers below and above. Such a metal-oxygen-metal trilayer is also charge neutral but has no dipole moment perpendicular to the surface, in contrast to a metal-oxygen *A*-*B* bilayer.

In short, for all the cubic iron oxides, the formation time of a new layer only depends on the number of cations per oxygen monolayer. This has been confirmed by quartz-crystal micro-balance measurements.[1] Consequently, for a fixed Fe deposition rate, the stoichiometry can be derived from the oscillation period. For example, in stoichiometric Fe_3O_4 and FeO, the cation densities are 8.51×10^{18} and 1.08×10^{19} $m^{-2}\,ML^{-1}$, respectively. Thus, going from Fe_3O_4 to FeO, the oscillation period will increase by a factor of 1.27.

In Ref. 38, we have described a convenient and very reproducible way to accurately determine these small variations in the oscillation period as a function of the growth conditions. By varying the NO_2 pressure while keeping the Fe flux constant, we can deposit many films with different stoichiometries on one and the same substrate. To ensure the same starting condition after each film, the sample has to be annealed in 10^{-6} Torr of oxygen for 1 h at 875 K. This treatment markedly flattens the surface resulting in very large (dimensions of $\sim$100 nm), flat and well-ordered terraces.[24,43] As demonstrated in Ref. 1, such ''recycled'' smooth surfaces enable one to observe strong RHEED oscillations upon further growth.

This experiment was performed for the present nitrogen-containing iron oxides. A selection of oscillation curves as a function of the NO_2 buffer volume pressure is shown in Fig. 11. All these oscillations were recorded with the electron beam incident along a [100] direction at an incidence angle of 0.68° (the anti-Bragg angle) and an electron energy of 15 kV. The intensity of the specular spot was determined by fitting the profile of a linescan perpendicular to the (0,0) surface diffraction rod. The best fits were obtained with Lorentz or Voigth curves. Plotted is the height of these curves, i.e., the background intensity has been subtracted.

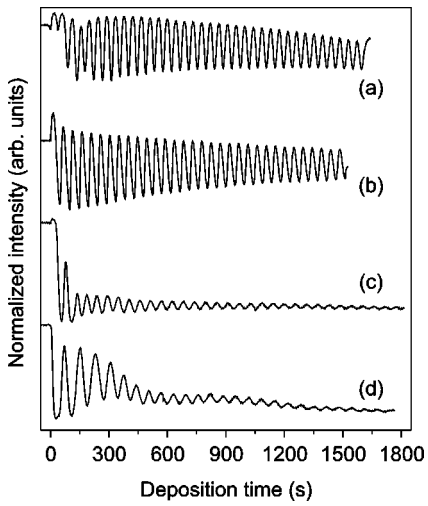

FIG. 11. RHEED intensity oscillations of the specularly reflected beam during deposition of nitrogen-containing iron-oxide films. All layers were grown on the same MgO(100) substrate by varying the NO_2 pressure while keeping the Fe flux constant. After each layer, the substrate surface was recovered by annealing. (a) Near-stoichiometric Fe_3O_4, 0.75-mTorr NO_2, (b) $Fe_{3+\delta}O_{4-y}N_y$, 45 mTorr, (c) $Fe_{1-x}O_{1-y}N_y$, 25 mTorr and (d) partially oxidized or metallic α-Fe, 15 mTorr. From the experimental ratio of the periods for Fe_3O_4 and $Fe_{3+\delta}O_{4-y}N_y$ or $Fe_{1-x}O_{1-y}N_y$, the value of δ or x can be calculated.

By combining the RHEED results with the XPS data, we have an elegant tool to determine the complete stoichiometry, *in situ*, and in a nondestructive way. In Table II, the RHEED periods of the low-flux films together with the nitrogen content from XPS and the resulting stoichiometry are listed as a function of the NO_2 pressure. From the CEMS spectrum, it can be derived that the 0.75 mTorr sample consists of stoichiometric Fe_3O_4 (see Ref. 1). Therefore, this sample was used as a calibration to determine the Fe content of the other samples. As a check, the RHEED period of a 1.00 mTorr sample, which is also stoichiometric Fe_3O_4 was measured. Within the error, i.e., 0.2 s, the same period was found.

When reducing the NO_2 flux, the oscillation period and therewith the iron content slowly increases up to 0.40 mTorr. This shows that not only stoichiometric Fe_3O_4 and $Fe_{1-x}O$ can be formed but also homogeneous solid solutions of these two phases. Initially, reduced magnetite is formed, which probably contains extra Fe interstitials (octahedral and/or tetrahedral). Although not in apparent contrast to the CEMS data, we find that also the 0.60 mTorr sample is slightly reduced.

Below 0.40 mTorr, the Fe content rapidly increases. Although the transition region is rather narrow, it appears that

TABLE II. Determination of the stoichiometry of wustite and magnetite films by combining the RHEED intensity oscillation periods and the nitrogen content from XPS. For the significance of the last two columns, we refer to the discussion in Sec. IV.

$p(NO_2)$ (mTorr)	RHEED period (s)	N/(N+O) from XPS	Composition	(N+O)/Fe	η
1.00	44.4		$Fe_{3.01}O_4$	1.33	
0.75	44.3		Fe_3O_4	1.33	
0.60	45.0		$Fe_{3.05}O_4$	1.31	
0.50	45.5	0.047	$Fe_{3.08}O_{3.81}N_{0.19}$	1.30	0.29
0.45	47.0	0.078	$Fe_{3.18}O_{3.69}N_{0.31}$	1.26	0.35
0.40	46.6	0.089	$Fe_{3.16}O_{3.64}N_{0.36}$	1.27	0.28
0.37	48.4		$Fe_{0.82}O_{1-y}N_y$		
0.35	50.6	0.13	$Fe_{0.85}O_{0.87}N_{0.13}$	1.18	0.37
0.30	57.3	0.14	$Fe_{0.97}O_{0.86}N_{0.14}$	1.03	0.39
0.25	56.8	0.17	$Fe_{0.96}O_{0.83}N_{0.17}$	1.04	0.36
0.20		0.18	$Fe_{1-x}O_{0.82}N_{0.18}$		

the change from magnetite to wustite is continuous. The period and the Fe content of a 0.37 mTorr sample at the boundaries of the $Fe_3(O,N)_4$ and $Fe_{1-x}(O,N)$ regions is in between those of the 0.40- and 0.35-mTorr samples. For 0.35 mTorr, we find an Fe content that agrees reasonably well with the RBS simulation [$Fe_{0.85}(O,N)$ vs $Fe_{0.82}(O,N)$, respectively].

Finally, phases are formed at 0.30 and 0.25 mTorr for which the oscillation period is nearly 1.27 times that of stoichiometric Fe_3O_4. This proves that these phases have the $\sim$1:1 wustite stoichiometry. For the 0.20-mTorr sample, we were not able to detect oscillations anymore. For even lower fluxes, the oscillations recurred. However, their period was very irregular, i.e., $\sim$77 s for the first few monolayers and subsequently $\sim$65 s [Fig. 11(d)]. This behavior is very similar to Fe deposited in a N_2O flux, and indicates the formation of metallic or only partially oxidized α-Fe; see Ref. 44.

From charge neutrality, it follows that in $Fe_{1-x}O$, the number of ferrous and ferric ions is given by $[Fe^{2+}]_{1-3x}[Fe^{3+}]_{2x}[O^{2-}]_1$. Similarly, for our oxynitrides $Fe_{1-x}O_{1-y}N_y$ we can write $[Fe^{2+}]_{1-3x-y}[Fe^{3+}]_{2x+y}[O^{2-}]_{1-y}[N^{3-}]_y$. Then, from the compositions given in Table II, we find Fe^{3+} fractions of 0.51, 0.21, and 0.26, for the 0.35–0.25-mTorr samples, respectively. These values differ to some extent from the ones obtained by CEMS. Nevertheless, both methods indicate that the nitrided wustite samples contain a larger amount of Fe^{3+} ions than pure $Fe_{1-x}O$.

IV. DISCUSSION

Although $Fe_{1-x}O$ is thermodynamically unstable below 833 K, its formation at low fluxes is not completely unexpected. As explained in the introduction, the oxidation with NO_2 is far away from equilibrium, and $Fe_{1-x}O$ films have also been grown with other, nonequilibrium MBE techniques. However, the phases we obtain at low fluxes are not pure oxides but are oxynitrides. As indicated by CEMS and XRD/RBS, they are remarkably stable. Even when exposed to air, the wustite sample prepared at 35 mTorr NO_2 maintains its structure and composition. The presence of nitrogen may help to stabilize the wustite for two reasons. First, it was found (see Sec. III C) that the lattice constant of unstrained $Fe_{1-x}O_{1-y}N_y$ is significantly smaller than that of pure $Fe_{1-x}O$, i.e., 0.4252(5) nm instead of 0.427 74–0.431 08 nm. Consequently, the lattice mismatch is reduced from approximately 2% to less than 1%. Therefore, the film will contain much less strain energy. Second, both CEMS and the RHEED oscillation periods indicate that $Fe_{1-x}O_{1-y}N_y$ has a larger Fe^{3+} fraction than pure $Fe_{1-x}O$. So, while the crystal structure is still similar to rocksalt, the oxidation state of the Fe ions actually resembles more the stable Fe_3O_4 phase. We speculate that this is a favorable factor too.

The cause of the nitrogen incorporation is obviously related to the use of NO_2 as the oxidizing agent. In particular, the almost linear increase of the nitrogen content with decreasing NO_2 flux gives a clear clue. In Ref. 1, it was found that NO_2 is a very efficient oxidizing agent. For preparing stoichiometric Fe_3O_4 films, it is sufficient that the fluxes of Fe and NO_2 are of the same magnitude, i.e., roughly every NO_2 molecule reacts with one Fe atom. Furthermore, it was found that all magnetite phases are pure oxides; no nitrogen could be detected in these films. These results show that at high fluxes, NO_2 exclusively acts as a source of oxygen. The simplest way to understand this is to assume that NO_2 dissociates at the surface into NO and atomically adsorbed oxygen.[45] The latter species then is responsible for the formation of the highly oxidized, nonstoichiometric magnetite phases up to pure γ-Fe_2O_3.

When the NO_2 pressure is reduced, at some point the flux of NO_2 molecules will be less than that of Fe. Presumably, this happens around 0.60 mTorr. From the geometry of our MBE setup, it can be calculated that at this pressure the fluxes of Fe and NO_2 are indeed of the same order of magnitude. Below 0.60 mTorr, the amount of atomic oxygen at the surface will be insufficient to fully oxidize all the metallic iron even if every NO_2 molecule dissociates and reacts. Consequently, some metallic iron would remain at the growing surface. We propose that this metallic iron reacts with

NO molecules adsorbed at the surface resulting in a partial incorporation of nitrogen into the samples. The abrupt start of the nitrogen incorporation contents suggest that the basic oxidation process is very efficient, i.e., only after all of the atomic oxygen has been consumed, the Fe starts to react with NO.

From the nearlinear increase of the nitrogen content with decreasing NO_2 flux, it can be deduced how NO reacts with Fe. The data indicate that of the remaining positions in the anion sublattice, on an average 66% are occupied by oxygen and the other 34% by nitrogen. In other words, not the entire NO molecule is consumed; it more often donates the oxygens than the nitrogens. To illustrate this, we do a calculation for the 0.50 mTorr sample. This sample has a composition of $Fe_{3.08}O_{3.81}N_{0.19}$ and therefore a ratio of N+O to Fe of 1.30. At 0.60 mTorr, this ratio is 1.31. These values are listed in the fifth column of Table II. If at 0.60 mTorr the amount of NO_2 is just sufficient to oxidize all Fe with atomic oxygen leaving the remaining NO unused, then at 0.50 mTorr, we have $0.50/0.60\times1.31=1.09$ NO_2 molecules per Fe. However, 1.30 are needed to build a complete anion sublattice. So, after oxidizing with all of the available atomic oxygens, there remains a fraction of 0.21/1.30 that has to be filled by NO molecules. From XPS, it is known that the nitrogen fraction is 0.047. Then, the fraction η of the remaining positions that is occupied by nitrogen follows from the equation $\eta\times0.21/1.30=0.047$, i.e., $\eta=0.29$. The values of η are listed in the last column of Table II. It can be seen that they are fairly constant with an average value of 0.34.

This model is supported by a sample prepared with NO as the oxidizing agent. We find that NO is indeed capable of oxidizing Fe and that the resulting phase is similar to the ones prepared at low NO_2 fluxes. However, NO is much less reactive than NO_2; a large excess (10.00 mTorr) is needed. RHEED and LEED patterns (not shown) indicated the formation of a magnetitelike phase. It had no $(\sqrt{2}\times\sqrt{2})R45°$ reconstruction and weak half-order spinel lines, similar to the 0.40 mTorr NO_2 sample. The CEMS spectrum is shown at the bottom of Fig. 10. Although the spectrum still has a sextet structure as of magnetite, there is also a clear paramagnetic component. From the RHEED period and XPS, it was deduced that this sample had an overall $Fe_{3.32}O_{2.88}N_{1.12}$ composition. This Fe content and the LEED, RHEED, and CEMS data indicate that this sample is very close or at the transition to wustite. The nitrogen fraction of 0.28 is in reasonable agreement with the fraction of 0.34, deduced from the NO_2 samples.

V. CONCLUSION

We have made an attempt to obtain the wustite $Fe_{1-x}O$ phase as epitaxial films on MgO(100) by applying the technique of NO_2-assisted MBE. When low fluxes of the oxidizing agent are used, the RHEED and LEED patterns indeed indicate the formation of a rocksalt-like structure. However, these samples are not pure oxides; they contain a small amount of nitrogen. Nonetheless, the XRD, RBS, and XPS spectra all indicate that the films are stable, single-phase crystals. From this fact, and from the BE of the N 1*s* peak in XPS, the weight of the nitrogen-related component in CEMS and the linear increase of the nitrogen content with decreasing NO_2 flux, it follows that the nitrogen atoms occupy substitutional sites of the oxygen-anion sublattice. In other words, the samples are oxynitrides. The composition of the wustite films can be written as $Fe_{1-x}O_{1-y}N_y$. Similarly, at slightly larger fluxes, we obtain reduced magnetites, which can be described as $Fe_{3+\delta}O_{4-y}N_y$. By combining the results of XPS and the RHEED intensity oscillation periods, we are able to obtain a complete picture of the stoichiometry of these samples.

The nitrogen uptake during growth can be explained with a simple model in which it is assumed that NO_2 molecules dissociate at the growing surface into atomic oxygen and molecular NO. The iron then first reacts with all of the available atomic oxygen before it starts to consume the NO. Although the model agrees well with our results, it is still speculative and should be verified by carrying out experiments to identify the various species at the growing surface.

ACKNOWLEDGMENTS

We thank Dieuwert Inia for performing the ERD measurements and Wilma Eerenstein for providing the LEED pattern of MgO. The technical assistance of Henk Bruinenberg is highly appreciated.

*Author to whom correspondence should be addressed. Present address: Philips Semiconductors, Proces en Materiaal Onderzoek (PMO), Building FB 0.099, Gerstweg 2, 6534 AE Nijmegen, The Netherlands. Electronic address: frans.voogt@philips.com

†Present address: Department of Applied Chemistry, Faculty of Engineering, Okayama University, Tsushima-naka 3-1-1, Okayama 700-0082, Japan.

[1] F.C. Voogt, T. Fujii, P.J.M. Smulders, L. Niesen, M.A. James, and T. Hibma, Phys. Rev. B **60**, 11 193 (1999).

[2] T. Fujii, D. Alders, F.C. Voogt, T. Hibma, B.T. Thole, and G.A. Sawatzky, Surf. Sci. **366**, 579 (1996).

[3] M.S. Seehra and G. Srinivasan, J. Phys. C **17**, 883 (1984).

[4] R.W.G. Wyckoff, *Crystal Structures*, 2nd ed. (Krieger, Malabar, FL, 1982), Vols. 1–3.

[5] W.K. Chen and N.L. Peterson, J. Phys. Chem. Solids **36**, 1097 (1975).

[6] C.R.A. Catlow and B.F.F. Fender, J. Phys. C **8**, 3267 (1975).

[7] F. Koch and J.B. Cohen, Acta Crystallogr., Sect. B: Struct. Crystallogr. Cryst. Chem. **25**, 275 (1969).

[8] T. Fujii, M. Takano, R. Katano, Y. Bando, and Y. Isozumi, J. Appl. Phys. **66**, 3168 (1989).

[9] M. Takano, T. Fujii, and Y. Bando, in *New Functionality Materials, Vol. C: Synthetic Process and Control of Functionality Materials*, edited by T. Tsuruta, M. Doyama, and M. Seno (Elsevier, New York, 1993), p. 745.

[10] R.M. Wolf, A.E.M. De Veirman, P. van der Sluis, P.J. van der Zaag, and J.B.F. aan de Stegge, in *Epitaxial Oxide Thin Films and Heterostructures*, edited by D.K. Fork, J.M. Philips, R. Ramesh, and R.M. Wolf, MRS Symposia Proceedings No. 341 (Materials Research Society, Pittsburgh, 1994), p. 23.

[11] C. Ruby, J. Fusy, and J.-M.R. Génin, Thin Solid Films **352**, 22 (1999).
[12] G.H. Vurens, M. Salmeron, and G.A. Somorjai, Surf. Sci. **201**, 129 (1988).
[13] G.H. Vurens, V. Maurice, M. Salmeron, and G.A. Somorjai, Surf. Sci. **268**, 170 (1992).
[14] W. Weiß and G.A. Somorjai, J. Vac. Sci. Technol. A **11**, 2138 (1993).
[15] W. Weiß, Surf. Sci. **377-379**, 943 (1997).
[16] S.B. Ogale, V.N. Koinkar, Sushama Joshi, V.P. Godbole, S.K. Date, A. Mitra, T. Venkatesan, and X.D. Wu, Appl. Phys. Lett. **53**, 1320 (1988).
[17] S. Yoshii, O. Ishii, S. Hattori, T. Nakagawa, and G. Ishida, J. Appl. Phys. **53**, 2556 (1982).
[18] C. Ortiz, G. Lim, M.M. Chen, and G. Castillo, J. Mater. Res. **3**, 344 (1988).
[19] Y.K. Kim and M. Oliveria, J. Appl. Phys. **75**, 431 (1994).
[20] Y. Gao, Y.J. Kim, and S.A. Chambers, J. Mater. Res. **13**, 2003 (1998).
[21] O.C. Rogojanu *et al*. (unpublished).
[22] A.V. Mijiritskii *et al*. (unpublished).
[23] F.C. Voogt, T. Hibma, G.L. Zhang, M. Hoefman, and L. Niesen, Surf. Sci. **331-333**, 1508 (1995).
[24] J.M. Gaines, P.J.H. Bloemen, J.T. Kohlhepp, C.W.T. Bulle-Lieuwma, R.M. Wolf, A. Reinders, R.M. Jungblut, P.A.A. van der Heijden, J.T.W.M. van Eemeren, J. aan de Stegge, and W.J.M. de Jonge, Surf. Sci. **373**, 85 (1997).
[25] T. Fujii, F.M.F. de Groot, G.A. Sawatzky, F.C. Voogt, T. Hibma, and K. Okada, Phys. Rev. B **59**, 3195 (1999).
[26] F.M.F. de Groot *et al*. (unpublished).
[27] W.M. Arnoldbik and H.H.M. Habraken, Rep. Prog. Phys. **56**, 859 (1993).
[28] J.H. Scofield, J. Electron Spectrosc. Relat. Phenom. **8**, 129 (1976).
[29] *Handbook of X-ray Photoelectron Spectroscopy*, edited by C.D. Wagner, W.M. Riggs, L.E. Davis, J.F. Moulder, and G.E. Muilenberg (Perkin Elmer, Eden Prairie, MN, 1979).
[30] E.Y. Jiang, D.C. Sun, C. Lin, M.B. Tian, H.L. Bai, and S. Liu Ming, J. Appl. Phys. **78**, 2596 (1995).
[31] C.A. Kleint, H.C. Semmelhack, M. Lorenz, and M.K. Krause, J. Magn. Magn. Mater. **140-144**, 725 (1995).
[32] D.T. Margulies, F.T. Parker, F.E. Spada, R.S. Goldman, J. Li, R. Sinclair, and A.E. Berkowitz, Phys. Rev. B **53**, 9175 (1996).
[33] F.C. Voogt, T. Hibma, P.J.M. Smulders, L. Niesen, T. Fujii, P.A.A. van der Heijden, R.J.M. van de Veerdonk, and P.J. van der Zaag, J. Phys. IV **7**, C1-601 (1997).
[34] K.-N. Tu, J.W. Mayer, and L.C. Feldman, *Electronic Thin Film Science for Electrical Engineers and Materials Scientists* (Macmillan, New York, 1992).
[35] I. Jackson, S.K. Khanna, A. Revcolevschi, and J. Berthon, J. Geophys. Res., [Oceans] **95**, 21 671 (1990).
[36] N.N. Greenwood and T.C. Gibb, *Mössbauer Spectroscopy* (Chapman and Hall, London, 1971).
[37] G.H. Wijnja *et al*. (unpublished).
[38] F.C. Voogt, T. Hibma, P.J.M. Smulders, and L. Niesen, J. Cryst. Growth **174**, 440 (1997).
[39] J.H. Neave, B.A. Joyce, P.J. Dobson, and N. Norton, Appl. Phys. A: Solids Surf. **31**, 1 (1983).
[40] B.A. Joyce, J. Electron Spectrosc. Relat. Phenom. **99**, 9 (1990).
[41] J. Zhang, J.H. Neave, B.A. Joyce, P.J. Dobson, and P.N. Fawcett, Surf. Sci. **231**, 379 (1990).
[42] M.A. James, F.C. Voogt, L. Niesen, O.C. Rogojanu, and T. Hibma, Surf. Sci. **402-404**, 332 (1997).
[43] J.F. Anderson, M. Kuhn, U. Diebold, K. Shaw, P. Stoyanov, and D. Lind, Phys. Rev. B **56**, 9902 (1997).
[44] F.C. Voogt, T. Hibma, P.J.M. Smulders, L. Niesen, and T. Fujii, in *Epitaxial Oxide Thin Films III*, edited by C. Foster, J.S. Speck, C.-B. Eom, and M.E. Hawley, MRS Symposia Proceedings No. 474 (Materials Research Society, Pittsburgh, 1997), p. 211.
[45] S.R. Bare, K. Griffiths, W.N. Lennard, and H.T. Tang, Surf. Sci. **342**, 185 (1995).